The Effect of Persistent Vortices on Boundary Layer Behavior in Turbulent Flow along a Kelvin-Stuart Cat's Eyes Wavy Wall

Amir Mehmedagic

A thesis submitted in partial fulfillment
of the requirements for the degree of

Master of Science in Aeronautics and Astronautics

University of Washington

2013

Committee:

Robert Breidenthal

Antonino Ferrante

Program Authorized to Offer Degree:

Department of Aeronautics and Astronautics

In presenting this thesis in partial fulfillment of the requirements for a master's degree at the University of Washington, I agree that the Library shall make its copies freely available for inspection. I further agree that extensive copying of this thesis is allowable only for scholarly purposes, consistent with "fair use" as prescribed in the U.S. Copyright Law. Any other reproduction for any purpose or by any means shall not be allowed without my written permission.

Signature_____

Date_____

TABLE OF CONTENTS

List of Figures iii

Chapter 1: Introduction 11

Chapter 2: Persistence Theory 12

Chapter 3: The Kelvin-Stuart Cat's Eyes Flow 15

3.1 Background ..…….... 15

3.2 The Separatrix and stability ……..……..... 17

3.3 Vortex translation and cross-flow ……... 18

Chapter 4: Experimental Setup 19

4.1 Wall Shape ..……..…… 19

4.2 Mechanical design ……..…….……..... 20

4.3 Vortex generators …….……..……... 20

4.4 Photographic setup……..…… 21

4.5 Hot-Film probe ……...……..……..... 22

4.6 Turbulence grid ……..... 22

4.7 Water tunnel ……..…….……... 23

Chapter 5: Experiment I: Boundary Layer Behavior 24

5.1 Finding the "sweet spot" …… 24

5.2 Comparison of persistent and non-persistent cases ...…..... 25

5.3 Results ……..……...…….……..... 25

5.4 Analysis and discussion …...…..……... 28

Chapter 6: Experiment II: Hot-Film Analysis 29

6.1 Hot-Film boundary anemometry ....…… 29

6.2 Results ……..……..…….……..... 30

6.3 Analysis and discussion ..……..……... 31

Chapter 7: Conclusions and Future Work 32

References 34

LIST OF FIGURES

Figure Number		Page
2.1	Entrainment diagrams illustrating different flow regimes	13
3.1	The regular pattern of the von Karman wake from flow around a bluff body	15
3.2	Cross flow field diagrams	16
3.3	Comparison of the new and previous wavy wall shapes used	16
3.4	Diagram illustrating the cross-flow component of the mainstream	18
4.1	Cat's Eyes shaped wavy wall hanging in the water tunnel	19
4.2	The backside of the wavy wall assembly	20
4.3	Illustration of the wavy wall apparatus with positive angle γ into the flow	21
4.4	Schematic of a Wheatstone Bridge	22
4.5	Adjustable turbulence grid	23
5.1	Stationary vortex core	25
5.2	Cat's Eyes wavy wall at ideal in 35cm/s	26
5.3	Turbulent boundary layer behavior in the non-persistent case	27
5.4	Boundary layer with turbulence grid upstream of cat's eyes wavy wall	27
5.5	von-Karman wavy wall at ideal settings in 35cm/s	28
5.6	Boundary layer with turbulence grid upstream of von-Karman wavy wall	28
6.1	Hot-wire data comparison	30

ACKNOWLEDGMENTS

I would like to thank Nicholas Harvey, my research assistant, for his invaluable help running these experiments, Professor Breidenthal for his encouragement, guidance and patience, Robert Gordon for his lab and equipment support, and my parents for their continued guidance and support in every single way along this long process.

Chapter 1

Introduction

Recent research performed by Balle and Cotel [1, 2, 3, 4, 5] have shown that the entrainment rate of large-scale vortices on a surface depend largely on the stationarity of said vortices relative to the surface; stationarity being defined as the ratio of the rotational to the translational velocity of the vortex relative to the surface. For a solid wall then persistence theory predicts that introducing a sufficiently strong, stationary vortex will reduce wall fluxes, such as heat transfer and skin friction, from turbulent to laminar values, even in initially turbulent flow. The work done by Dawson and Bauer [4,5] has shown successful boundary layer relaminarization using a wavy wall shaped like the separatrix of a von Karman wake in order to maintain vortex stationarity. They also noticed that the flow more closely resembled a Kelvin's Cat's Eyes flow, which this study aims to use to achieve better boundary layer relaminarization.

If persistence theory proves to be accurate, applications could be widely implemented. Systems could be devised that would protect solid walls from very hot flows in jet turbines or rockets, space re-entry vehicles, potentially even plasma engines or fusion reactors. The speed and efficiency of watercraft could also be greatly increased by reducing skin friction of hulls. Ultimately if a reliable enough system is created skin friction on aircraft could be significantly reduced. While not fully tested, work done by Prateek Ranjan using a wing with a wavy upper surface showed potential to greatly increase the stall angle of the wing, while only increasing drag by a much smaller amount than predicted.

Chapter 2

Persistence Theory

The experiments and theory by Cotel, Breidenthal, et al. [1, 3, 4, 5], that were the basis for persistence theory, showed that entrainment rates across stratified surfaces were not only affected by the usual parameters Richardson number (*Ri*), Reynolds number (*Re*), Prandtl (*Pr*), and Schmidt (*Sc*) numbers as stated in Taylor's entrainment hypothesis [7] , but also by vortex persistence along the surface. They introduced this new fundamental parameter (T) defined as

$$T \equiv \frac{W}{V \cdot \pi} \tag{2.1}$$

Where W is the azimuthal velocity of the vortex and V is its translational velocity relative to the nearby surface. It can be noted that the persistence parameter approaches infinity for a perfectly stationary vortex. While not accounted for in equation 2.1, the relationship between W and V is directly affected by the strength of the stationary vortex as described in Chapter 3; therefore as shown in [5,6] vortex strength is an additional criterion of the persistence parameter.

Figure 2.1 shows the results of experiments performed by Cotel *et al.* on the effect of all the parameters, including persistence, on the entrainment rate. It is evident that the entrainment regimes are drastically affected by the transition from a non-persistent to a persistent vortex at T_{cr}. Breidenthal explains figure 2.1 as:

Figure 2 is an entrainment diagram of the model for the nonpersistent limit, where T is less than some critical value T_{cr}, of order unity. For simplicity, the Schmidt number is assumed to be greater than unity, and the interface is thin. In each regime, the normalized entrainment rate is given, to within a dimensionless coefficient. A single line between regimes indicates a continuous transition, while a double line indicates a discontinuous transition.

For example, if $Ri > Re^{1/4}$, the entrainment rate is independent of Ri and proportional to $Re^{-1/4}$. This is the smooth "flat interface" regime, where the stratification is so great that even the smallest turbulent eddies have insufficient kinetic energy to engulf a tongue of fluid across the interface… All fluxes here must be diffusive, since Roshko's entrainment tongues are absent.

Figure 3 is the corresponding entrainment diagram for the persistent limit, $T > T_{cr}$. Note that the entrainment rate for the flat interface regime now depends on the square root of the Reynolds number, a laminar flux, even though the flow is turbulent at large Re.

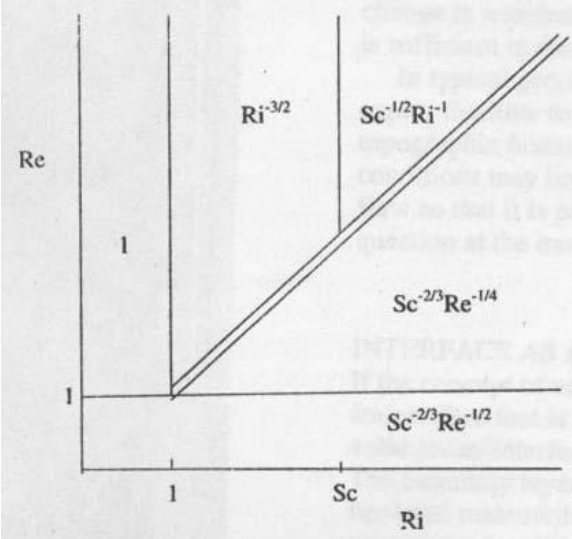

Figure 2. Entrainment diagram, $T < T_{cr}$

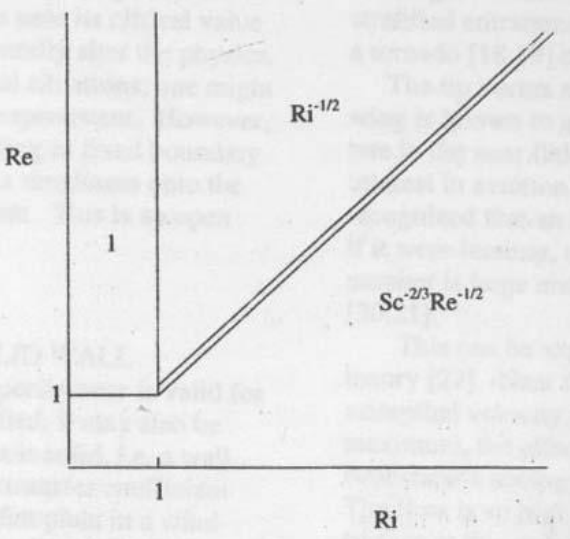

Figure 3. Entrainment diagram, $T > T_{cr}$

Figure 2.1: Entrainment diagrams illustrating different flow regimes

As the Ri number becomes very large, i.e. the surface becomes solid, even the smallest eddies are unable to pull tongues of fluid across the stratified surface; therefore the fluxes across this

surface must be purely diffusive [5], proportional to the square root of the ratio of the diffusivity (D) to the time scale of the rate-limiting eddy (τ_λ) in the turbulent cascade:

$$\omega_e = \left(\frac{D}{\tau_\lambda}\right)^{\frac{1}{2}} \tag{2.2}$$

The largest eddies mainly transport large fluid elements over large distances and to the smaller scales, while the smallest eddy scales (Kolmogorov scale) are effective at generating new surface area and molecular mixing. If the large eddies are non-persistent then the diffusive fluxes are generated by the smallest eddies, and diffusive fluxes become high. When the largest vortices are persistent, then they become the rate-limiting eddy, and due to their longer rotation period the diffusive fluxes decline to laminar values since the fine-scale turbulence no longer determines the diffusivity. As Balle stated [10] "Physically speaking, while the large-scale eddies persist in the same location, i.e. are stationary, the small scales are 'starved' of new fluids to mix at the molecular scale…" In the limit of a solid wall ($Ri \to \infty$), the surface must have purely diffusive fluxes, as should the boundary layer, both of which should decline to laminar values under a persistent vortex.

Balle and Toule [10, 11] discovered that the surface heat flux values from a heater mounted to the backside of a wavy wall, modeled after the von Karman vortex street, reduced from turbulent to laminar values by an order of $Re^{\frac{1}{4}}$ when persistent vortices were held in the troughs of the wavy wall, in accord with persistence theory. Olivia Dawson [7] further showed, using visual analysis of dye injections near a larger scaled wavy wall, that the boundary layer was significantly (~50% of the surface) relaminarized when strong, stationary vortices was present in the troughs of the wavy wall. Matthias Bauer [8] repeated Dawson's experiment using hot-film anemometry to obtain quantifiable data on the boundary layer turbulence, and found similar results of approximately 95% reduction in flow intermittency (turbulence) over about half of the surface.

Chapter 3

The Kelvin-Stuart's Cat's Eyes Flow

3.1 Background

Balle and Kier [9, 10] were the first to maintain vortex stationarity near a solid surface using a wavy wall based on the separatrix of the von Karman vortex street. This vortex pattern is created by the shedding that occurs behind a bluff body in low Reynolds number flow (Fig. 3.1). This vortex arrangement was found to be a stationary solution and at least quasi-stable [Dawson].

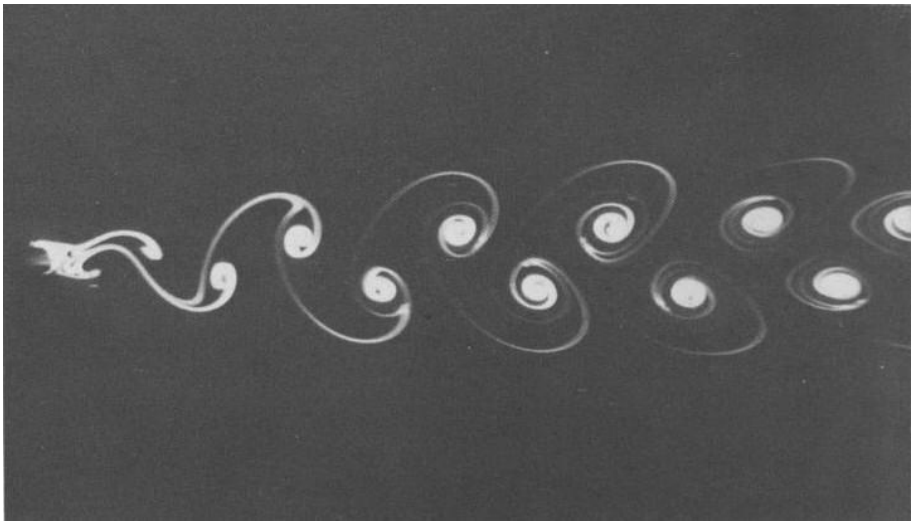

Figure 3.1: The regular pattern of the von Karman wake from flow around a bluff body [12]

Although Balle mentions that there are other vortex patterns that could be used to achieve stationarity, the von-Karman wavy wall (approximated using corrugated sheet metal) was used exclusively to study persistence, until Dawson concluded by mapping the flow field that the flow more closely resembled the Kelvin's cat's eyes pattern (Fig. 3.2). She hypothesized that making

the crests of the von Karman wavy wall come to a point may eliminate the awkward flow region atop the crests and give better results. Bauer attempted to more accurately match the separatrix of the Cat's Eyes flow by welding sharp crests to the tops of Dawson's von-Karman wavy wall. However due to the bump in the surface created by the welding, and not fully matching the Cat's Eyes separatrix his relaminarization results were only slightly better than Dawson's, if not the same. It is difficult to accurately compare visual analysis with hot-film data.

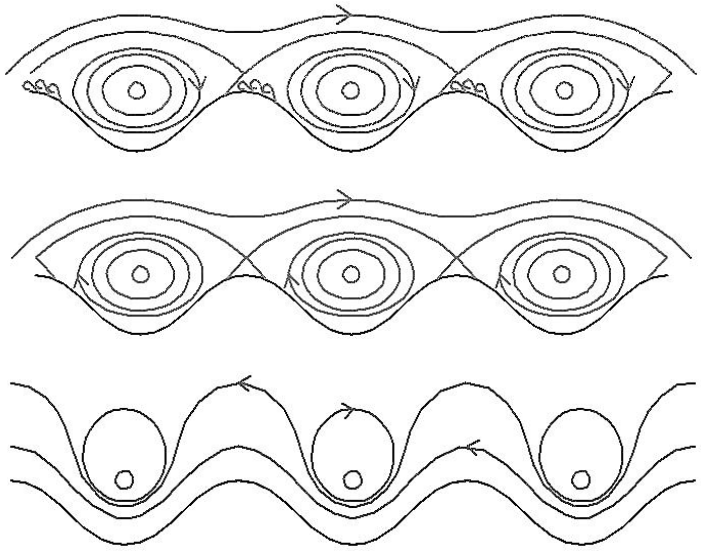

Figure 3.2: Above: A sketch of the instantaneous flow field made from flow visualization. Center: A time averaged view of the field. Below: A sketch of the von Karman potential streamlines for comparison.

For this study a custom made wall surface was shaped to match the separatrix of a Kelvin-Stuart Cat's Eyes flow that is stable to linear and non-linear perturbations (See Fig. 3.3).

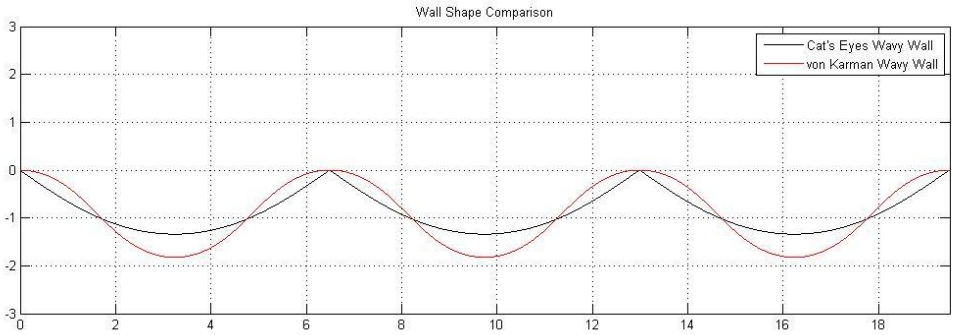

Figure 3.3: Comparison of the new and previous wavy wall shapes used

3.2 The separatrix and stability

Holm, Mardsen and Ratiu [19] studied the linear and non-linear stability of the cat's eyes flow, specifically the stationary solution of Kelvin (1880)-Stuart (1967). The shape of the streamlines is given by

$$y = \cosh^{-1}\left(\frac{e^{\Psi} - \sqrt{a^2-1}\cos x}{a}\right) \tag{3.1}$$

where Ψ represents the streamlines, and (a) is a real shape parameter, satisfying $a \geq 1$, that gives the thickness of the cat's eyes flow. Unlike the fixed aspect ratio of the von-Karman vortex street [7, 10], this shape factor has a range of values; however an upper limit can be derived in order for the cat's eyes flow to maintain linear and non-linear stability

$$\left(a - \sqrt{a^2-1}\right)^2 > \frac{2l^2}{\pi^2 + l^2} \tag{3.2}$$

where l is a function of (a) and Ψ. This inequality is derived for a domain involving a single period, or eye, of $[0, 2\pi]$. If the separatrix is used as the y-boundary of the domain then this inequality holds for

$1 \leq a \leq 1.175$	for a single period (eye) $[0,2\pi]$
$1 \leq a \leq 1.153$	for two periods $[0,4\pi]$
$1 \leq a \leq 1.136$	for the desired three periods $[0,6\pi]$

Using this final maximum value of (a) a solid wall can be designed using Eq. 3.1 to replace the separatrix streamline with theoretically no effect in potential flow. The three stationary vortices can then be generated at the centroid of each trough or eye as was done for the previous experiments.

In order to compare visual and hot-wire data with Dawson and Bauer's work the distance between peaks, or wavelength, was maintained at 6.5" (165 mm), which gave an a amplitude of 1.34" (34mm). This amplitude is almost a half inch "shallower" than the wavy wall previously used, the effect of which is discussed in Chapter 7.

3.3 Street translation and cross-flow

As with the von-Karman vortex street the Cat's Eyes flow also has a constant translational velocity with respect to the freestream fluid. This translational velocity is given by

$$U_{street} = \frac{\Gamma}{2a}\tanh\frac{\pi h}{a} \tag{3.3}$$

where Γ is the circulation of the vortex, and h and a are the amplitude and wavelength of the trough respectively. For this and previous wavy wall experiments the apparatus turns the orientation of the cat's eyes wake on its side, so that an array of half-delta wings generate vortices at the centroids of the wavy wall, so that the flow can be analyzed along the length of the vortex cores as they travel along their individual streamwise trough of the solid surface.

This orientation of the wavy wall induces this U_{street} component perpendicular to the freestream. In order to maintain the vortices in the centroids of the troughs, and therefore persistence, as the vortices travel downstream along the surface the wavy wall must be angled to the freestream. Fig. 3.4 describes this geometric relationship and Fig. 4.1 shows it being implemented in the water tunnel.

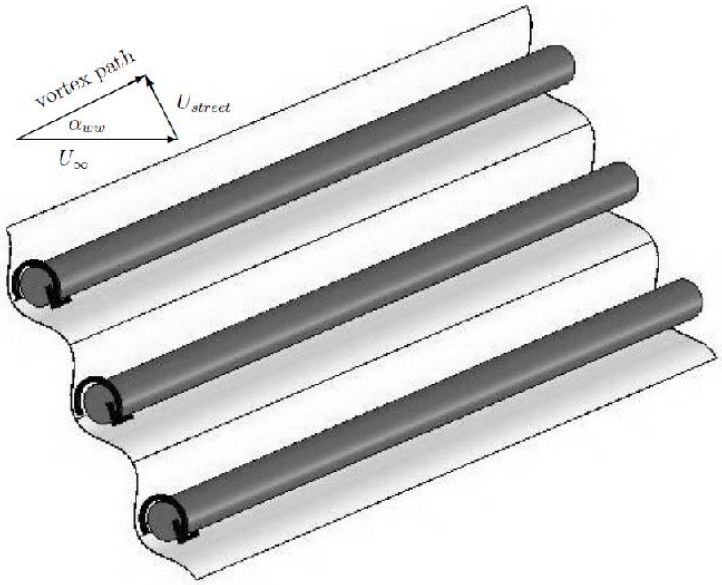

Figure 3.4: Diagram illustrating the cross-flow component of the mainstream.

Chapter 4

Experimental Setup

4.1 Wall shape

The experimental setup for this study is based on several previous experiments performed by Balle, Dawson and Bauer [7, 8, 10]. The difference being that the wavelength of the wall is larger than the one used by Balle, and matches Dawson and Bauer's experiments; however as previously stated the shape of the wavy wall does not match the von-Karman vortex street that Dawson used, but rather follows the Kelvin-Stuart Cat's Eyes flow as Bauer attempted to recreate, but to a higher degree of accuracy (see Fig. 4.1).

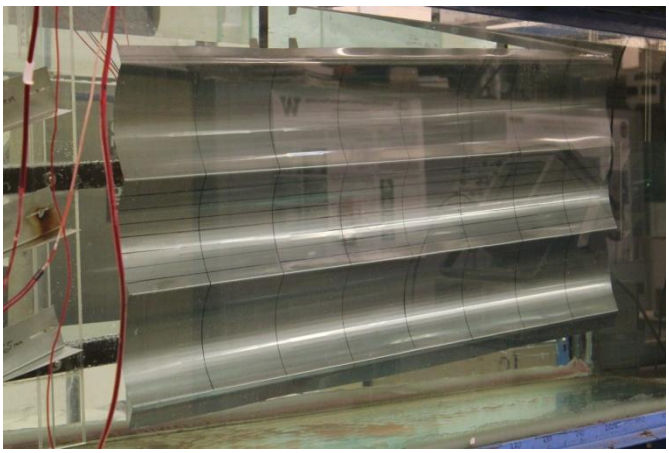

Figure 4.1: Cat's Eyes shaped wavy wall hanging in the water tunnel

The larger wavelength allows an increased optical resolution as well as higher attainable Reynolds numbers. The tests were run from 9-35 cm/s of freestream velocity, which correlate to $Re \approx 15{,}000 - 58{,}000$, based on the walls wavelength. The cat's eyes shape allows for better

contouring of the flow geometry, and therefore potentially better relaminarization results. The surface is constructed from a stainless steel sheet formed using a breaking apparatus to incrementally bend the sheet at set intervals in order to match the exact shape of the stable Kelvin-Stuart Cat's Eyes separatrix as described by Eq. 3.1 and shown in Fig. 3.3.

4.2 Mechanical design

The wavy wall is mounted in the test section of the water tunnel so as to give it four degrees of freedom. The surface hangs by two assemblies attached to leadscrews, as shown in Fig. 4.2, which allow the surface to be moved in both directions perpendicular to the flow, as well as rotations in yaw angle γ, as described in Fig. 4.3 and more importantly pitch angle α_{ww}, as illustrated in Fig. 3.4, in order to match the U_{street} and attain vortex persistence along the length of the surface.

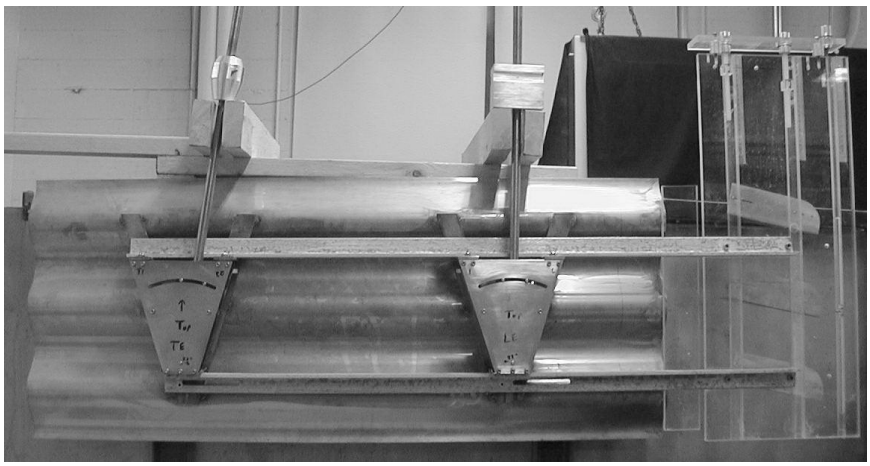

Figure 4.2: The backside of the wavy wall assembly. The trapezoidal aluminum assemblies contain pivoting mechanisms. The solid aluminum fixtures from which it is suspended provide the necessary degrees of freedom to allow pitch and yaw into the flow

4.3 Vortex generators

An array of three half-delta vortex generators (VG's) is positioned in front of the wavy wall's leading edge; each VG produces a streamwise vortex at the centroid of each trough. The array is mounted on a plate with two slides that allow the leading and trailing edges to be moved

independently, thus allowing the VG position and angle of attack (vortex strength) to be changed. VG size is related to the vortex depth within the trough, and several different sizes of VG's were tested in order to find the optimum vortex position. It should be noted that because the VG's are mounted to the wavy wall's brackets, their angles of attack are directly correlated by

$$\alpha_{total} = \alpha_{ww} + \alpha_{vg} \tag{4.1}$$

where α_{total} is the VG angle of attack to the freestream, α_{vg} is the angle of the VG's relative to the array plate on which they are fixed, and α_{ww}, as stated previously, is the angle of the wall with respect to the surface of the water. Because of this correlation the fine tuning of the wall and VG's must be done carefully in order to maintain constant vorticity.

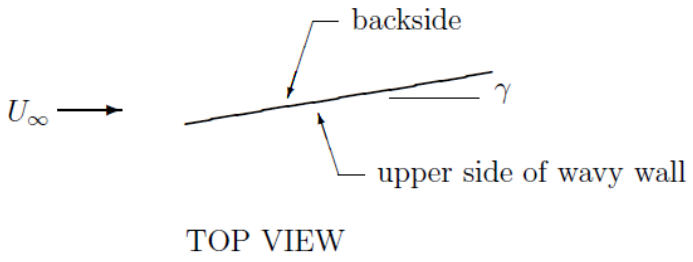

Figure 4.3: Illustration of the wavy wall apparatus with positive angle γ into the flow

4.4 Photographic setup

The flow was visualized using an array of dye injectors with alternating red and blue colored dye. In order to observe the boundary layer behavior, dye was injected into the flow through small holes drilled into the surface of the wall at various locations along a cross section of the middle trough, at three wavelengths downstream of the leading edge. All flow visualization was performed on the middle vortex. Dye was also injected at the apex of the VG in order to visualize the behavior of the vortex core.

All digital photographs were recorded with a 2012 Cannon EOS Rebel T2i DSLR camera, using a Canon Telephoto Lens: EF70-200mm, and a Circular Polarizer filter to minimize glare from the glass and water.

4.5 Hot film probe

The nonsteady velocity inside the boundary layer was measured using hot film anemometry in order to corroborate visual analysis, and to compare to hot film data obtained by Bauer on the previous wall shape. The Nusselt and Reynolds numbers are used to relate heat transfer observed by the probe to flow speed. The hot film's resistivity is a function of its temperature, which is maintained by a Wheatstone Bridge (see Fig. 4.4) by adjusting the voltage through the hot film. Higher flow speed leads to an increased cooling of the hot film and subsequently a higher voltage through it in order to maintain temperature. This adjustment can be made extremely quickly, in the range of micro- and nano- seconds, so a broad range of velocity frequencies can be measured. The probe used in this experiment was a TSI MODEL 1212-20W. The data was collected at a sampling rate of 200 Hz and 400Hz in order to compare results.

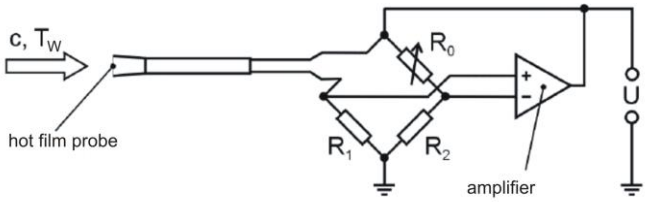

Figure 4.4: Schematic of a Wheatstone Bridge

4.6 Turbulence grid

Varying levels of turbulence were introduced in the freeflow upstream from the wavy wall assembly using an adjustable grid with removable bars (see Fig. 4.5), in order to test the ability of the wavy wall to relaminarize already turbulent flow. Turbulence intensity at the leading edge of the wavy wall can be calculated using Equation 4.2:

$$\frac{k}{U_0^2} = A\left(\frac{d}{M}\right)^{-n} \tag{4.2}$$

where k is the turbulent kinetic energy, U_0 is the freestream velocity, A varies widely depending on the geometry and Reynolds number, d is the distance from the grid, n is a constant that has been found to equal 1.3, and M is the grid spacing [16]. M ranged from 4.67" up to 14", and d was kept constant at 48".

Figure 4.5: Adjustable turbulence grid.

4.7 Water tunnel

All experiments were conducted in a water tunnel with a test section of 28” x 28” (70 cm x 70cm). The freestream velocity used ranged from 0-35cm/s, and was controlled by an electronically-controlled pump with an input in units of Hz. The pump and controller are calibrated in order to correlate the controller’s Hz input with actual flow speed.

Chapter 5

Experiment I: Boundary Layer Behavior

5.1 Finding the "sweet spot"

Before the boundary layer could be analyzed, the "sweet spot" of the apparatus had to be found which positioned a strong enough stationary vortex within the wavy wall trough in order to achieve persistence. Although, as mentioned previously, this study is based on previous experiments by Dawson and Bauer with a similar wavy wall, the fundamental change in the shape of the wavy wall as well as the construction process used to create the new apparatus significantly altered the ideal settings in order to achieve persistence.

An iterative process very similar to Dawson's [7] was used in order to achieve persistence. This was done by fixing the pitch angle of the wavy wall (α_{ww}), and then varying the position and angle of attack of the VGs (α_{vg}) until the vortex core dye stream remained along the centerline of the trough with a minimum oscillatory motion in its travel downstream (see Fig. 5.1). This process also helped determine the tolerance or size of this "sweet spot" within which persistence was still achieved. This method was then iterated over a range of different VG span sizes. The span determines the height of the vortex above the trough, and the same persistence "sweet spot" criteria were used for each VG.

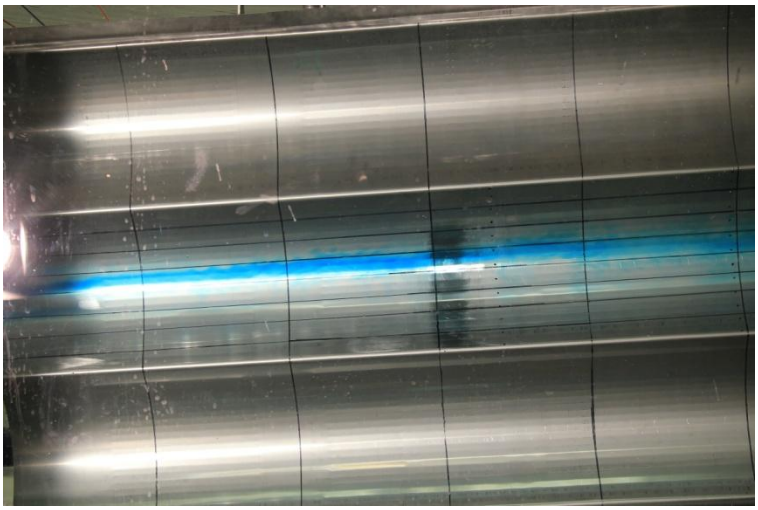

Figure 5.1: Stationary vortex core

5.2 Comparison of the persistent and non-persistent cases

Persistence theory, as defined so far, predicts that in the presence of a strong, stationary vortex wall fluxes decrease to their laminar values, even if the boundary layer is initially turbulent. The boundary layer behavior was visualized with red and blue dye injected through the wall surface at five locations across the middle trough, at three wavelengths downstream of the leading edge of the wall.

At lower flow speeds the boundary layer tended to relaminarize under all circumstances, so final testing was done at 35 cm/s in order to have an initially turbulent boundary layer, and the predictions of persistence theory could be properly tested. The turbulence grid was also used with different numbers of bars so that the relaminarization of freestream turbulence could also be explored.

5.3 Results

The optimal settings determined for 35cm/s that gave the stationary vortex seen in Fig. 5.1 were:

VG semi-span: 70mm

VG leading edge station on array plate: 96mm

VG trailing edge station on array plate: 60mm

$\alpha_{ww} = 3.1°$

$\alpha_{vg} = 15.8°$

$\alpha_{total} = 18.9°$

This shows a significant increase in vortex strength needed in order to maintain persistence compared to the von Karman shape used by Dawson and Bauer; however the "sweet spot" was found to also be significantly larger. Dawson noted that "a slight change in VG angle (less than half a millimeter's translation of the leading edge) can result in an observable change in the vortex core's behavior." The cat's eyes shaped wall could handle a couple of millimeter's translation of the leading edge. It was also less sensitive to changes in VG location, and could handle translation by about 5mm compared to the 2 mm found by Dawson.

The boundary layer at the ideal settings mentioned above is shown in figure 5.2. There was a cyclic instability in this boundary layer behavior from a secondary vortex that builds up on the VG over several seconds and is then shed downstream. This secondary vortex build up was also observed by Dawson and Bauer, and is a known feature of flow over delta wings.

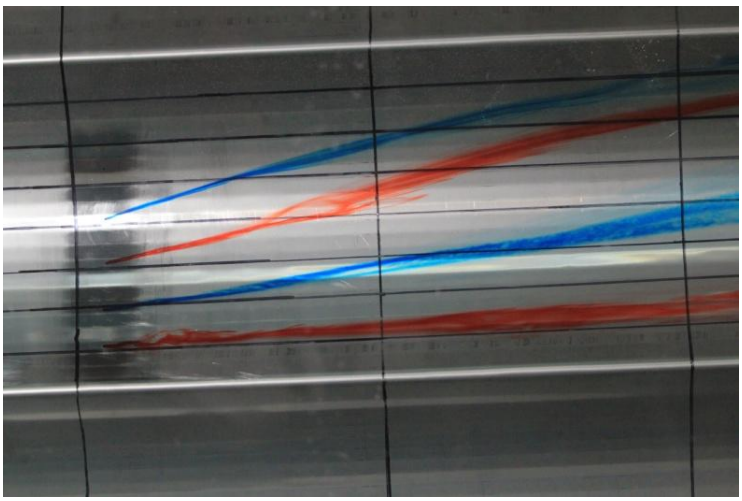

Figure 5.2: Cat's Eyes wavy wall at ideal in 35cm/s

As mentioned above the sweet spot where persistence is maintained was found to be larger than with the previous wall shape; however when outside of this sweet spot vortex breakdown occurs

and the boundary layer returns to turbulent. Figure 5.3 shows this turbulent behavior when the VG is translated above the ideal location by 10 mm. Similar boundary layer behavior was also observed when the VG angle and the wall pitch angle were changed from the ideal location.

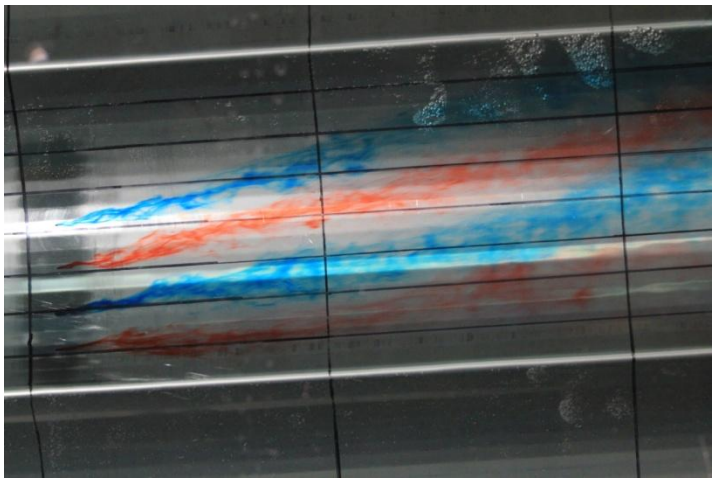

Figure 5.3: Turbulent boundary layer behavior in the non-persistent case

In the persistent case at the ideal settings and in the presence of freestream turbulence created using the turbulence grid the laminar boundary layer was maintained throughout the various grid spacings used. The cyclic instability from the secondary vortex periodically shed off the VG became more pronounced as more turbulence was present in the boundary layer. Figure 5.4 shows the laminar boundary layer achieved, as well as the short burst of turbulent flow.

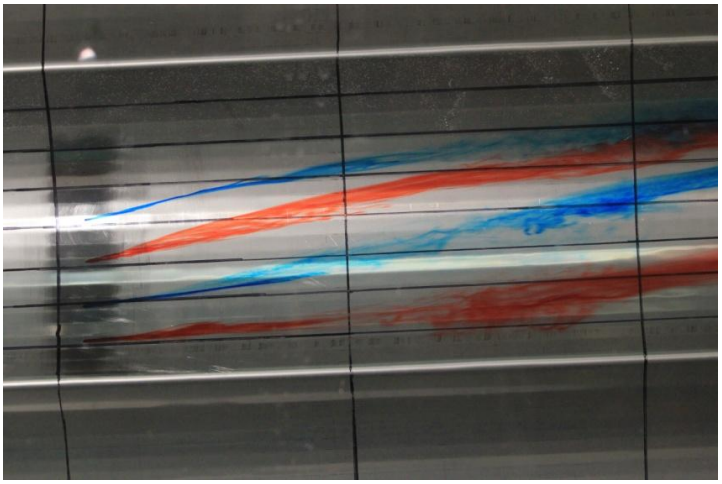

Figure 5.4: Boundary layer with turbulence grid (M=4.67) upstream of cat's eyes wavy wall

5.4 Analysis and discussion

As expected persistence theory was once again proven to dominate wall fluxes, and as hypothesized a wall shape more closely matching the Kelvin's Cat's Eyes flow separatrix allowed for a significantly more stable system. When compared to the boundary layer of the von Karman shaped wall at the ideal settings found by Dawson (see Fig. 5.5), it is visually evident that a much larger percentage of the wall surface is kept laminar with the cat's eyes wavy wall.

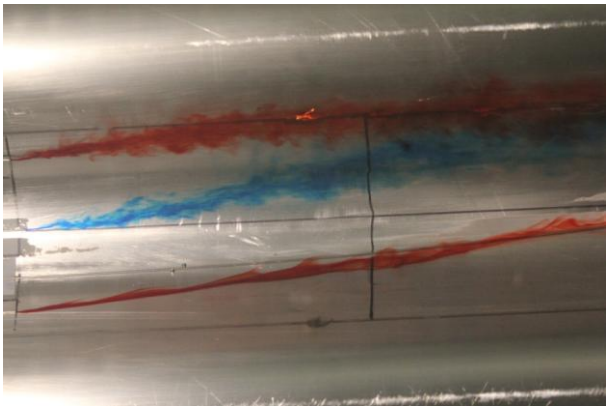

Figure 5.5: von-Karman wavy wall at ideal settings in 35cm/s

Similar performance improvements were found when the turbulence grid was used to introduce turbulence in the freestream flow. Figure 5.6 shows some relaminarization of the boundary layer by the von Karman wavy wall; however as can be observed in Figure 5.4 above, the persistent vortex had a much stronger effect on the cat's eyes wavy wall, which had stronger relaminarization characteristics.

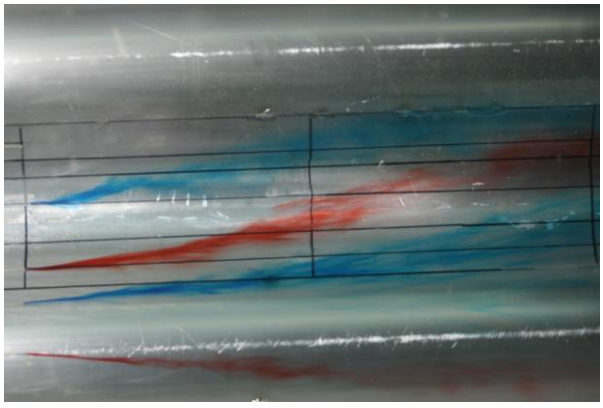

Figure 5.6: Boundary layer with turbulence grid (M=4.67) upstream of von-Karman wavy wall

Chapter 6

Experiment II: Hot-Wire Analysis

6.1 Hot-wire anemometry

Hot-wire anemometry of the boundary layer was performed in order to quantitatively confirm qualitative results found in the previous chapter. As stated previously, Bauer [8] focused on hot-wire analysis of the von Karman wavy wall used by Dawson in order to quantify her visual results. A similar approach to Bauer's was used in this experiment to gather and analyze hot-wire data using Reynolds triple decomposition (Eq. 6.1) of the hot-wire signal using a self-made MATLAB code.

$$u(t) = \bar{u} + \tilde{u}(t) + u(t)' \tag{6.1}$$

where $\bar{u}$ is the average signal value, $\tilde{u}(t)$ is the periodic fluctuation of the probe, and $u(t)'$ represents the turbulence. The periodic fluctuation of the probe (not part of the flow) is taken out of the whole signal using a bandpass filter in the code, after frequency analyzing the entire signal, using Fourier Transforms, to find the range of the usable frequency band (7-60Hz). The voltage data from the hot-wire was finally boiled down to an intermittency factor:

$$\delta = \frac{\sum t_{turbulent}}{\sum t_{total}} \tag{6.2}$$

which is defined as the fraction of time the flow is turbulent. The turbulence condition was determined locally, for every 40 points, in the signal from the frequency filtered signal using a global threshold (Eq. 6.3) derived for each test point.

$$X = v'_{min} + k \cdot (v'_{max} - v'_{min}) \tag{6.3}$$

where v' is the root mean square value of the $u(t)'$ values from the decomposed signal, and (k) is a factor that allows adjustment of the threshold. A range of values for k were tried out a value of 0.14 gave a good decomposition of the signal into its laminar and turbulent segments. The hot-wire analysis was performed at five wavelengths downstream from the LE in order to have comparable data to Bauer's.

6.2 Results

Figure 6.1 shows the intermittency factor at the thirteen test points across the middle trough under ideal persistence conditions as described in Chapter 5. On the middle and right sides of the trough (pos. 5-13) the flow is laminar over 99% of the time. From position 5 to 1, the flow then becomes increasingly turbulent.

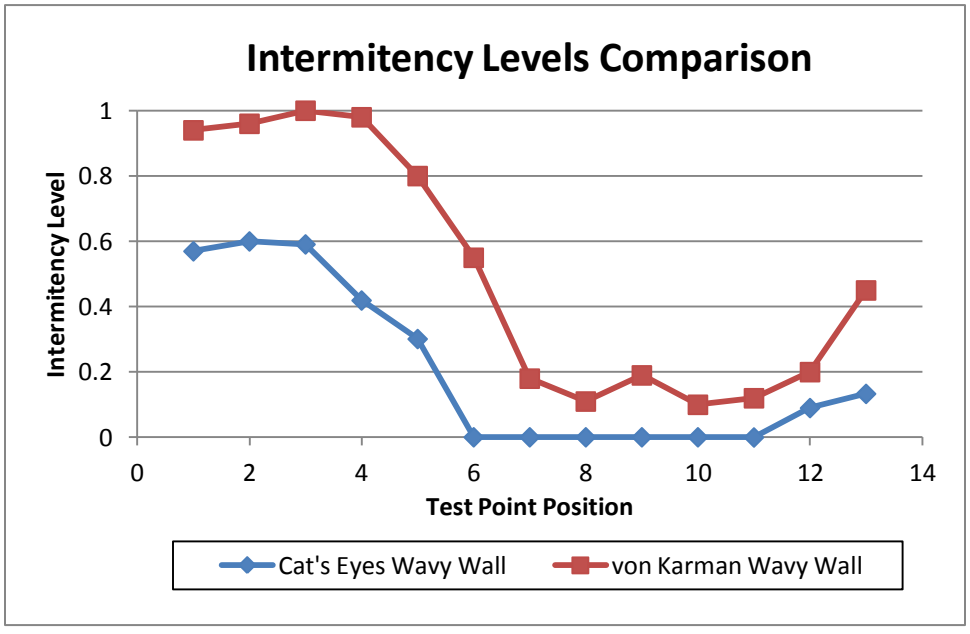

Figure 6.1: Hot-wire data comparison

6.3 Analysis and discussion

When compared to Bauer's boundary layer data in Figure 6.1 for the von Karman wavy wall with added peaks, the hot-wire data taken with the cat's eyes wavy wall shows a wider relaminarization area, as well as much lower intermittence levels in the turbulent section of the trough. The left side of the trough has an adverse pressure gradient associated with the vortex pulling away from the wall's surface, which is believed to cause the increase in turbulence in that region; however because the shape of the cat's eyes wavy wall more closely matches the flow field in this adverse region the area under turbulence is significantly smaller than with the previously used von Karman wavy wall, as well as having lower intermittency levels.

Chapter 7

Conclusions and Future Work

The flow visualization and hot-wire results of this study further support persistence theory: the behavior of a boundary layer along a solid wavy wall is controlled by the presence of a persistent vortex. The domination of wall fluxes by a strong, stationary vortex forces an initially non-laminar boundary layer to become laminar. Even varying intensities of upstream turbulence, generated by the adjustable grid, had minimal impact on the relaminarized boundary layer. This is very promising for future research in potential real world applications of persistence theory.

Replacing the von Karman potential flow dividing streamline with the Kelvin-Stuart Cat's Eyes separatrix as the shape for the solid wall showed improved relaminarization characteristics, and more stable persistent vortices. When looking at the flow field it was evident that the stagnation areas to the left and bottom of the vortex seen in Figure 3.2 were much less prominent using this new wall shape.

The increased relaminarized surface area, and decrease in intermittency levels in the turbulent area, as well as the decrease in total wetted surface area due to shallower waves opens up more potential applications. Wing dynamics with an integrated wavy upper and/or lower surface need

to be explored. This type of system could potentially replace riblets which function at the Kolmogorov scale and are adversely affected by contaminants such as small dirt particles. The shorter rotation periods of riblets only offer modest drag reductions, of order 10% [20], where as the experiments with persistence theory have demonstrated an order of 50-60% drag reduction, this effect being larger at higher Reynolds number. Higher Reynolds numbers also need to be explored in order to have practical applications on planes, watercraft hulls, rocket and jet engines as mentioned in the introduction.

Overall drag reduction of the entire system is also an area of potential study. While there is an obvious drag benefit from the relaminarized boundary layer, the system must invest energy into the vortex creation. It is important to note that for a lifting wing, the more important goal is higher L/D. Since lift and drag are both adversely affected by flow separation, there may be a net benefit associated with implementing a wavy wing surface, even with the cost of utilizing vortex generators.

In the experiments performed so far on persistence theory using wavy walls, only passive controls have been used to achieve and maintain persistence, which has greatly limited the size of the "sweet spot" and therefore the applicability of persistence theory. While there is a benefit to only having a mechanical system (less complex, more reliable), the potential of using active controls on the various wall and VG angles to better maintain persistence should be explored.

References

[1] A.J. Cotel and R.E. Breidenthal. Persistence theory of stratified entrainment. In *Fourth International Symposium on Stratified Flows*, Grenoble, 1994.

[2] G.J. Balle. Stationary vortices and persistent turbulence in karman grooves. *Journal of Turbulence*, 3(033), 2002.

[3] A.J. Cotel, J.A. Gjestvang, N.N. Ramkhelwan, and R.E. Breidenthal. Laboratory experiments of a jet impinging on a stratified interface. *Experiments in Fluids*, 23:155-160, 1997.

[4] A.J. Cotel and R.E. Breidenthal. A model of stratified entrainment using vortex persistence. *Applied Scientific Research*, 57:349-366, 1997.

[5] R.E. Breidenthal. Turbulent stratified entrainment and a new parameter for surface fluxes. *Recent Res. Devel. Geophysics*, 2:61-65, 1999.

[6] R.E. Breidenthal. A new parameter for vortices near interfaces - the vortex persistence. In *35th Aerospace Sciences Meeting & Exhibit, Reno, NV*, volume 97-0437. AIAA, January 6-10 1997.

[7] O.R. Dawson. The effect of persistent vortices on boundary layer behavior in flow along a wavy wall. Master's thesis, University of Washington, 2005.

[8] M Bauer. Boundary layer turbulence measurements near a persistent streamwise vortex. Project report, University of Washington, 2006.

[9] Theimo Matthias Kier. Vortex behavior near a corrugated wall. Master's thesis, University of Washington, 1999.

[10] G.J. Balle. *Stationary Vortices and Persistent Turbulence*. PhD thesis, University of Washington, 2001.

[11] H. Touel. Turbulent wall fluxes with stationary vortices. Technical report, Department of Aeronautics and Astronautics, University of Washington, June 1999.

[12] Milton van Dyke. *An Album of Fluid Motion*. The Parabolic Press, Stanford, CA, 1982.

[13] N.E. Kochin, I.A. Kibel, and N.V. Roze. *Theoretical Hydrodynamics*. Interscience, New York, 1964.

[14] P.G. Saffman. *Vortex Dynamics*. Cambridge University Press, Cambridge, 1992.

[15] J.D. Anderson. *Fundamentals of Aerodynamics.* McGraw-Hill, New York, 2nd edition, 1991.

[16] Stephen B. Pope. *Turbulent Flows.* Cambridge University Press, Cambridge, 2000.

[16] Hermann Schlichting, Klaus Gersten, E. Krause, H. Jr. Oertel, and K. Mayes (Translator). *Boundary-Layer Theory.* McGraw-Hill, New York, 7th edition, 1979.

[17] D. Oster and I. Wygnanski. The forced mixing layer between parallel streams. *Journal of Fluid Mechanics,* 123:91-130, 1982.

[18] F.A. Roberts. *Effects of a periodic disturbance on structure and mixing in turbulent shear layers and wakes*. PhD thesis, California Institute of Technology, 1985.

[19] Darryl D. Holm. Nonlinear stability of the Kelvin-Stuart Cat's Eyes Flow. *Lectures in Applied Mathematics.* Volume 23, 1986.

[20] Bushnell DM, Hefner JN. Viscous drag reduction in boundary layers. *Progress in Astronautics and Aeronautics*, 123.